Single and multiple muon events in the LVD detector

Anzivino, G.; Bianco, S.; Casaccia, R.; Cindolo, F.; Felice, M. De; Enorini, M.; Fabbri, F.L.; Laakso, I.; Pallante, E.; Susinno, G.

Published in:
Nuclear Instruments and Methods in Physics Research A

DOI:
10.1016/0168-9002(90)90728-O

Publication date:
1990

Nuclear Instruments and Methods in Physics Research A295 (1990) 466–476
North-Holland

Single and multiple muon events in the LVD detector

G. Anzivino, S. Bianco, R. Casaccia, F. Cindolo, M. De Felice, M. Enorini, F.L. Fabbri, I. Laakso, E. Pallante, G. Susinno, L. Votano and A. Zallo
INFN, Laboratori Nazionali di Frascati, P.O. Box 13, 00044 Frascati, Italy

G. Bari, M. Basile, G. Bruni, G. Cara Romeo, L. Cifarelli, A. Contin, C. Del Papa, P. Giusti, G. Iacobucci, G. Maccarrone, T. Massam, R. Nania and G. Sartorelli
Dipartimento di Fisica and INFN, Sezione di Bologna, Bologna, Italy

G. D'Alì
Dipartimento di Fisica dell'Università, Palermo, Italy

A. Zichichi
CERN, Genève, Switzerland

Received 20 April 1990

Expected rates of deep-underground muons in the LVD detector, at a vertical depth of 3600 hg/cm^2 s.r. (standard rock) at the Gran Sasso, were obtained through Monte Carlo simulation. Two different generators were developed to reproduce single and multiple muon distributions at our detector level. The main purpose was to evaluate the potentiality of the apparatus in studying chemical composition and energy spectra of primary cosmic rays in the range 10^{14}–10^{16} eV through the detection of muon bundles of high multiplicity. Sensitivity of the detector was checked by comparing event-rate predictions for three different models of the primary composition: the Maryland spectrum, the "low energy composition" model, and the NUSEX parametrization (with spectral index of iron $\gamma_{Fe} = 2.60$ and 2.70). We predict a single muon rate in the apparatus of about 3.26×10^6 events/year. Preliminary results for multiple muon-event detection show that we can separate with a good sensitivity different primary compositions in the multiplicity region around $n = 10$.

1. Introduction

In the most recent years significant results were obtained in the study of high-energy cosmic-ray muons from indirect measurements in underground experiments. At present, multipurpose detectors with a very large sensitive area, located at large depths, can easily gain orders of magnitude in the observed rates of single and multiple muons in a reasonably short time of operation.

Muons observed deep underground are the high-energy remnants of atmospheric showers originated in the first collisions of the primary nuclei with the air nuclei. As a result, muon rates are sensitive both to primary composition and energy spectrum and to the properties of hadronic interactions.

At energies around 10^{12} eV primary flux is essentially due to five components: protons, α-particles, CNO group, the Si–Mg group and the iron group. Single muons are mainly produced by light components, protons and helium, with energies $\sim 10^{13}$ eV. At higher energies the contribution from high multiplicities to the underground muon flux increases, with an increasing contribution of heavier nuclei.

Two main aspects of cosmic-ray behaviour need still to be cleared up. The first one is the evidence that at energies around 10^{15} eV/nucleon (the so-called "knee region") the energy spectrum for the five components becomes steeper. A possible explanation of this effect could involve a reduced efficiency of the magnetic fields in the confinement of primary nuclei in our Galaxy. The second one concerns the experimental evidence of a steady increase of the fraction of heavy nuclei up to $\sim 10^{14}$ eV.

Because of the very low flux of the primaries in the most interesting ultrahigh-energy range ($E \approx 10^{14}$ eV), direct measurements are not easily accessible. In this respect, multiple muon physics deep underground be-

0168-9002/90/$03.50

comes the best indirect way to investigate primary flux at energies $> 10^{14}$ eV. On the other hand, the fundamental problem of this kind of measurement, mostly inherent in any indirect measurement, is the large number of parameters involved in extrapolating the observed rates, angular distributions and spectra of secondary muons to the primary flux and composition. Uncertainties and possible discrepancies in experimental results become strongly dependent both on the model adopted for the high-energy hadronic interactions and on the precision with which all the experimental conditions (geometry of the detector and triggering requirements, mountain shape and rock composition) are known.

At the simulation stage we developed a set of Monte Carlo generators of single and multiple muon events for studying our detector response and accurately estimating its sensitivity to the primary spectra. The evidence that we can easily have access to multiplicities ≥ 10 is a very favourable condition and will allow to reach significant conclusions on the primary cosmic-ray behaviour above the "knee region" and high-energy hadronic interactions in the near future.

2. Overview of the detector

The LVD multipurpose detector is located in the Gran Sasso laboratory, hall A, at a vertical depth of 3600 hg/cm^2 s.r. It has a modular design. Each module contains two independent systems for event detection: a liquid scintillator system and a tracking system with limited streamer tubes. The two main aims of the experiment are: (i) the study of the neutrino interactions inside the detector; energy measurement, for low-energy neutrino interactions, and pattern identification for higher-energy neutrino-induced events, (ii) through going-muon detection, with track reconstruction, up–down discrimination and time-of-flight measurement.

The whole structure consists of 190 almost identical modules (6.3 m × 2.6 m × 1.1 m each) divided in five adjacent towers. We summarize in table 1 the main characteristics of the detector structure (total dimensions and weight), including the total number of active nuclei in liquid scintillator.

Table 1
Characteristics of the LVD detector

Dimensions	$(40\times12\times13)$ m^3
Total weight	3600 ton
Scintillator mass	1800 ton
Active nuclei in scintillator:	
free protons	1.7×10^{32}
electrons	6.4×10^{32}
^{12}C nuclei	7.4×10^{31}

Each module houses the liquid scintillator system of eight counters (1 m × 1.5 m × 1 m each), filled with C_nH_{2n+2} ($n = 10$) and the tracking system, with limited streamer tubes grouped in an L-shaped double layer on one side and bottom of the module. Each layer has an independent system of pickup strips, parallel to the tubes (X strips) and transverse to the tubes (Y strips) for the readout of the two plane coordinates.

The basic element of the tracking layer consists of an extruded PVC open profile (6.2 m long) divided in eight cells (cross section 9 × 9 mm^2) with 1 mm separation walls and coated with graphite (cathode resistivity ≥ 50 kΩ/square). The diameter of the silver-plated Be–Cu anode wire is 100 μm. The whole system is inserted in an uncoated PVC container 1 mm thick. The gas mixture used is the standard one (argon/isobutane 30/70).

3. Depth calculation

We describe the effective rock thickness above the apparatus, in a direction with polar angles (θ, ϕ), through the function $h(\theta, \phi)$, which has to be numerically evaluated for a given site. For slant depth calculation we have used a digitized map [1] of the Gran Sasso in the zone above the laboratory tunnel. Contour lines [illegible] with step [illegible] in height on a total area of ~ 500 km^2.

The data are converted in slant thickness values $h(\theta,\phi)$, for fixed direction (θ, ϕ) in the upper hemisphere, through a bidimensional linear interpolation [2] between adjacent contours. The table of values generated is a 45 × 72 matrix: 45 points in zenithal angle θ, on the interval 0–90°, with step $\Delta\theta = 2°$, and 72 points in azimuthal angle ϕ, from 0° to 360°, with step $\Delta\phi = 5°$. A standard rock density of $\rho = 2.65$ g/cm^3 was assumed in the present calculation.

4. Single muons

4.1. Monte Carlo simulation

Underground measurements of single muon rates give directly the intensity curve $I(h, \theta)$ at the detector level for accessible intervals Δh, $\Delta\theta$ of slant depth and zenithal angle. The observed vertical intensity–depth curve is then related to the muon energy spectrum at sea level $J(E_\mu)$ through the survival probability function as follows:

$$I(h) = \int_{E_{th}} P(E_\mu, h) J(E_\mu)\, \mathrm{d}E_\mu, \qquad (1)$$

where E_μ is the initial energy of the incoming muon and E_{th} is the energy threshold corresponding to a survival

probability, at a depth h, $P(E_{th}, h) = 0$. The exact knowledge of the survival probability $P(E_\mu, h)$ becomes a very crucial point in propagating high-energy muons through the surrounding rock * (the energy threshold E_{th} corresponding to a survival probability of 1% is 1.2 TeV in vertical direction at the Gran Sasso laboratory [3]).

For what concerns the simulation we distinguish three different classes of parameters. They define: (i) mountain geometry and composition, (ii) characteristics of the detector, shape and trigger efficiencies, (iii) all the physical mechanisms involved in secondaries generation and propagation. While the first two points require a detailed reproduction of the experimental conditions, the last one can be known in an independent way and few sets of parametrizations are now available both from Monte Carlo simulation and experimental data.

Single muon distributions at the depth of the detector are perfectly determined if we know two functions:

i) the intensity–depth relation $I(h, \theta)$, which gives the single muon flux as a function of depth and angle;
ii) the differential energy spectrum at the detector level.

Possible parametrizations of $I(h, \theta)$ and muon energy spectrum at sea level $J(E_\mu)$ result from analysis of event rates of different underground experiments operating in the last few years: NUSEX [4] and the spark chamber experiment [5] (Garage 27) in the Mt Blanc laboratory, the Utah experiment [6], Kolar gold field [7] and the French–US Collaboration [8] in the Mt Blanc tunnel. We referred to the data from NUSEX and Garage 27 experiments in the present Monte Carlo simulation. Our generator performs single track generation in two steps:

4.1.1. A direction is extracted with the weight function $I(h, \theta)$

The depth interval we are interested in is approximately 3600–10000 hg/cm^2. An extended and consistent range of data for the intensity–depth curve is that from NUSEX and Garage 27. They give the most recent parametrization in the two ranges 3900–7100 hg/cm^2 (from Garage 27) and 5000–10000 hg/cm^2 (from NUSEX experiment) in perfect agreement with each other. The parametrization we have used is

$$I(h, \theta) \approx A h^{-a} e^{-bh} \sec\theta \quad \text{cm}^{-2}\,\text{s}^{-1}\,\text{sr}^{-1}, \tag{2}$$

with $A = 108.5$, $a = 2.51$, $b = 7.177 \times 10^{-4}$ hg^{-1} cm^2 for $h < 5000$ hg/cm^2, and

$$I(h, \theta) \approx I_0 e^{-h/h_0} \sec\theta \quad \text{cm}^{-2}\,\text{s}^{-1}\,\text{sr}^{-1}, \tag{3}$$

with $I_0 = 7.63 \times 10^{-7}$ cm^{-2} s^{-1} sr^{-1}, $h_0 = 810.44$ hg/cm^2, for $h > 5000$ hg/cm^2.

Approximating the angular dependence with the "sec θ law" we have only considered the "conventional" muon contribution from $\pi^\pm$ and $K^\pm$ decay. This is a reasonable assumption for an event-rate prediction, according to the NUSEX results [4], which estimate a contribution to the vertical muon intensity from "prompt" muons (produced in charmed mesons decay) less than 4% of the total one.

4.1.2. Muon energy at the detector level is extracted knowing the energy spectrum as a function of depth

The differential energy spectrum $J(E_f, h)$ for muons with final energy E_f at slant depth h, is related to the surface spectrum $J(E_i)$ as follows:

$$J(E_f, h) = \int_0^\infty J(E_i) f(E_f, E_i, h)\, dE. \tag{4}$$

The function $f(E_f, E_i, h)$ takes into account energy losses, including the effects of range fluctuations for muons of TeV energies. We note that, if the intensity–depth curve is expressed as

$$I(h) = \int_0^\infty J(E_f, h)\, dE_f$$

$$= \int_0^\infty dE_f \int_0^\infty J(E_i) f(E_f, E_i, h)\, dE_i, \tag{5}$$

comparing with eq. (1) for $I(h)$, the survival probability function can be related to the function f as follows:

$$P(E_i, h) = \int_0^\infty dE_f f(E_f, E_i, h). \tag{6}$$

In a low-energy approximation all the fluctuations are negligible and the exact range–energy relation holds; $f(E_f, E_i, h)$ is now a $\delta(E_f - \mathbb{E}_f(E_i, h))$ function. In this case the known parametrization for the energy loss function $\mathbb{E}_f(E_i, h)$ in the hypothesis of null fluctuations is valid:

$$E_f = \mathbb{E}_f(E_i, h) = (E_i + \epsilon)\, e^{-bh} - \epsilon. \tag{7}$$

Assuming a power-law spectrum at sea level, $KE_i^{-\gamma}$, we finally have

$$J(E_f, h) = K\, e^{-bh(\gamma-1)} \left[E_f + \epsilon(1 - e^{-bh})\right]^{-\gamma}. \tag{8}$$

An appropriate parametrization of the range–energy relation, from simulation results given by Gaisser and Stanev [9], takes roughly into account the effects of the range fluctuations through the rock for muons with energy $E_\mu \geq 1$ TeV. We have used their results taking the values $\epsilon = 530$ GeV and $b = 4 \times 10^{-4}$ hg^{-1}cm^2. For the sea-level muon energy spectrum parameters we assumed the values $K = 19.17$ and $\gamma = 3.71$ from Garage 27 results [5].

* At TeV energies the muon energy loss is dominated by the processes of bremsstrahlung and e^+e^- pair production, which introduce large fluctuations in the survival probability. As a consequence the range–energy relation becomes not unequivocal and $P(E_\mu, h)$ is no more a Θ-function.

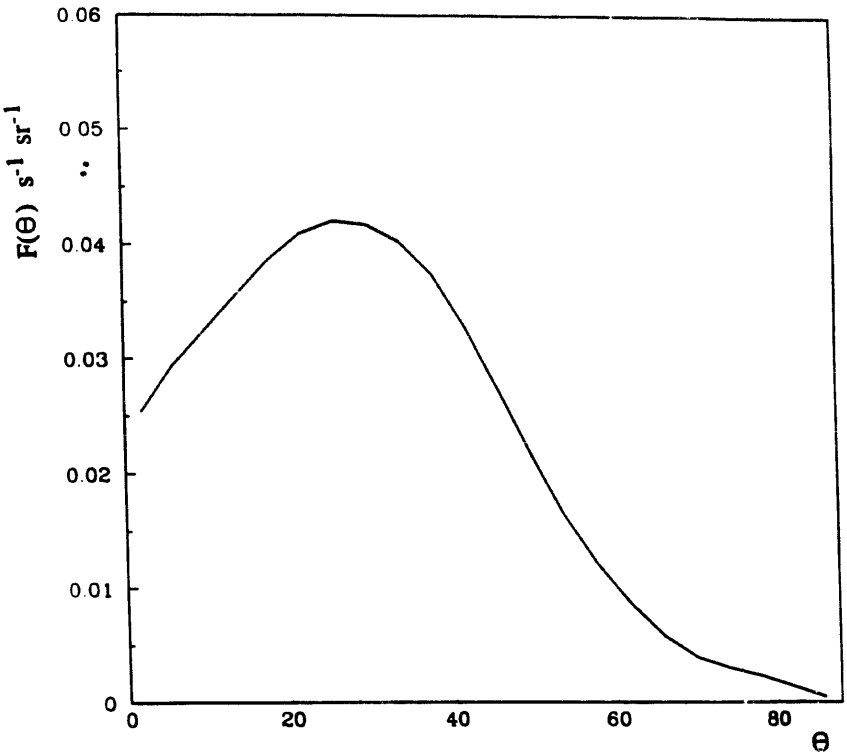

Fig. 1. Predicted zenithal distribution of single muon rate for the LVD detector.

4.2. Rate of single muon events in the LVD

The total rate of single muon events in the apparatus is given by the relation

$$R = \int_{\Omega} I(h(\omega), \theta) S(\omega)\, d\omega \quad s^{-1}, \tag{9}$$

where the integration of the incoming flux $I(h, \theta)$ is done over the whole solid angle seen by the detector, weighted with the "directional response function" $S(\omega)$. In the simplest case, for detectors of regular shape, $S(\omega)$ can be analytically expressed. If we define an "ideal detector" as a box with the outermost dimensions of the LVD, the response function is simply expressed through the formula

$$S_{box}(\omega) = S_x |\cos\phi| \sin\theta + S_y |\sin\varphi| \sin\theta + S_z |\cos\theta|. \tag{10}$$

The second step is to include the real configuration of the whole internal structure of the detector and the trigger logic definition, for tracks selection and reconstruction. In this more general condition, $S(\omega)$ can become a complicated function of the event direction and an alternative way of calculation is needed. We have performed a full preliminary and separated Monte Carlo simulation to obtain the detector response including all triggering requests. The logic we adopted for track selection is the following:

- Form a *plane signal*: logical AND of the two adjacent layers (horizontal or vertical) in the same module.
- Form a *superplane signal*: logical OR of coplanar plane signals contained in two adjacent towers.
- Form the *trigger*: the coincidence of at least two superplane signals.

The total trigger efficiency is 69.5% for the physical distribution of downward single muons. Details of the analysis are described in refs. [10,11]. As a result we reproduce the directional response function $S(\omega)$ in terms of a "grid of acceptance": a table of numerical values of the sensitive detector surface as a function of polar angles, with steps $\Delta\theta = 2°$ and $\Delta\phi = 5°$.

The expected total rate of single muons was finally obtained through numerical integration of eq. (9). Our prediction for the LVD is

$R = 3.26 \times 10^6$ events/year

A total flux per unit area of 0.78 muons/(m^{2}h) is obtained. In fig. 1 the predicted rate of single muon events is shown as a function of the zenithal angle θ. The maximum corresponds to about 26° of inclination from the vertical.

5. Muon bundles

5.1. Monte Carlo simulation

Understanding muon bundles is one of the current problems of cosmic-ray physics in underground experiments. Although the large number of parameters required for the analysis of experimental results is a

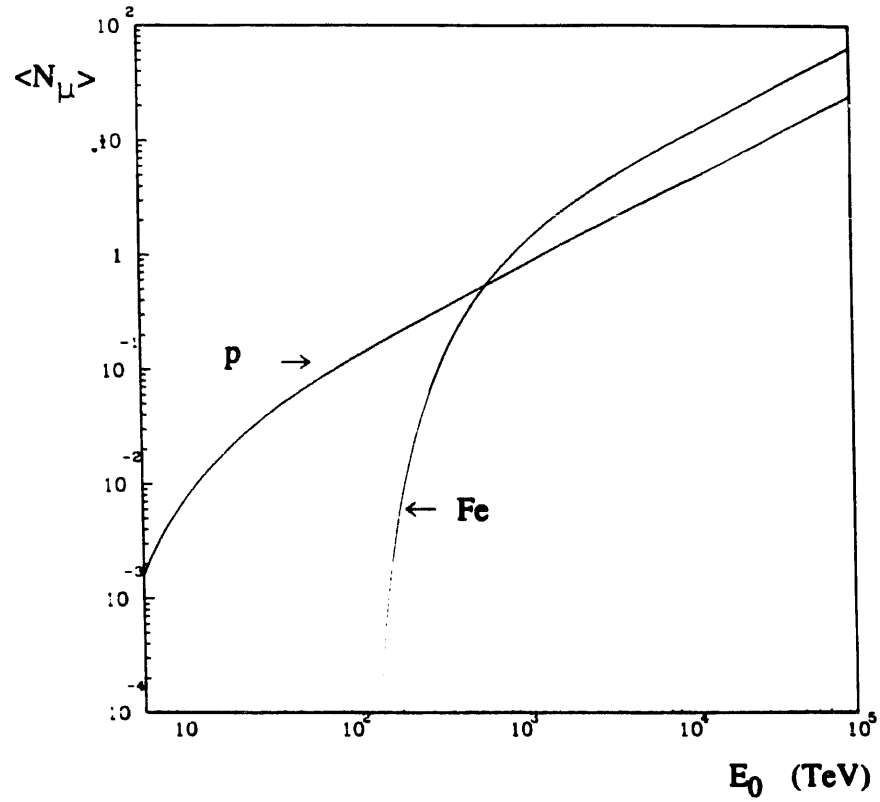

Fig. 2. The average muon multiplicity in a bundle as a function of the total energy of the primary component calculated for protons and iron nuclei at a vertical depth of 4000 hg/cm^2 s.r., using the parametrization (13), from ref. [13].

source of uncertainties, this kind of measurement remains a very likely way to access primary energies $> 10^{14}$ eV. On the other hand, both the predictions and extrapolations from experimental data to the primary flux are strongly model dependent. The development of extensive air showers (EAS), whose high-energy muon content we observe deep underground, requires assumptions on nucleus–air interaction far above 1 TeV.

Close to laboratory energies of 10^{15} eV informations on nucleon–nucleon interaction behaviour (multiplicity distributions, charged multiplicity dependence of the average transverse momentum $\langle p_t \rangle$ and the "seagull" effect) come available from recent data at the CERN $p\bar{p}$ collider [12] (up to $\sqrt{s} = 900$ GeV), while the energy region up to 10^{16} eV is not yet covered by measurements. Present models for cosmic-ray propagation through the atmosphere operate for this reason with minimal extrapolation up to these energies in describing hadronic interactions.

Sensitivity of multiple-muon rates to the primaries composition arises from the fact that a different average event multiplicity originates from nuclei of different mass at the same total energy. As shown in fig. 2, heavier nuclei become more efficient in high-multiplicity event production with increasing total energy. Therefore the most favourable experimental condition has to guarantee high sensitivity of the detector to high multiplicities (this essentially means $n > 6$, where no observations are present up to now).

Our calculation of event rates R_n, with observed multiplicity n, essentially proceeded through two main steps:

1) Calculation of the muon bundle flux at the detector level as a function of the primary nucleus energy E_0, the average mass A of the primary, the slant depth $h(\theta, \phi)$ in a given direction and the muon energy threshold $E_\mu(h(\theta, \phi))$ (which is a function of slant thickness).
2) Folding in the detector. Because of the finite size of the apparatus the observed number of muons in a bundle can be sensibly reduced from the real one, depending on the muon lateral spread. The effect in our detector has been measured through the calculation of a probability function $P_n(N)$ of detecting $n \leq N$ muons out of N muons in the bundle.

5.1.1. Multiple muon flux

The primary spectrum can be described as a superposition of power-law energy spectra:

$$\frac{dN}{dE_0} = \sum_i K_i(A) E_0^{-\gamma_i(A)} \quad \text{cm}^{-2}\,\text{s}^{-1}\,\text{sr}^{-1}\,\text{GeV}^{-1}, \tag{11}$$

where the summation is over the five primary compo-

nents (p, He, CNO, Mg, Fe), $K_i(A)$ is a coefficient depending on the normalization energy in the range of direct measurements and $\gamma_i(A)$ is the spectral index.

We define the directional muon flux at the depth of the detector for a given true multiplicity N as

$$\Phi_N(\Omega) = \sum_i K_i(A) \int E_0^{-\gamma_i(A)} \times P_N(E_0, A, E_\mu(h(\Omega)), \theta)\, dE_0, \quad (12)$$

where we have introduced the probability for a primary nucleus of energy E_0 and average mass A to generate a bundle of multiplicity N, with energy $\geq E_\mu$, present at slant depth h in a given direction Ω.

This probability function is completely determined once the interaction model is defined and the configuration of the rock burden is known. For calculations we have used the results from Monte Carlo simulations [13] firstly developed by Elbert and then adapted to NUSEX experimental site by Gaisser and Stanev. The assumptions are:

– the $\langle N \rangle$ function for the average number of muons with energy $> E_\mu$ from a primary component of energy E_0 and mass A can be parametrized as follows:

$$\langle N \rangle (E_0, A; > E_\mu) = \frac{A}{E_\mu} G(E_\mu, E) \sec\theta, \quad (13)$$

with

$$G(E_\mu, E) = 0.0145 \left(\frac{E}{E_\mu}\right)^{0.757} \left(1 - \frac{E_\mu}{E}\right)^{5.25}$$

(E, E_μ in TeV),

$$E_\mu\ [\text{TeV}] = 0.53(e^{0.4h} - 1) \quad (h \text{ in km w.e. (water equivalent)}),$$

and $E = E_0/A$ is the energy per nucleon.

– the actual N distribution around $\langle N \rangle$ can be well described as Poissonian. Therefore the probability $P_N(E_0, A, E_\mu(h(\Omega)), \theta)$ is given by

$$P_N(\langle N \rangle) = \frac{\langle N \rangle^N}{N!} e^{-\langle N \rangle}, \quad (14)$$

with $\langle N \rangle$ from eq. (13). Nevertheless, on the basis of the last results from the $p\bar{p}$ collider, most recent Monte Carlo calculations [3] for atmospheric cascade suggest a multiplicity distribution around the mean value better described by a negative binomial distribution and take into account the charged multiplicity dependence of the average transverse momentum $\langle p_t \rangle$.

A useful expression of the flux $\Phi_N(\Omega)$ is the following [14]:

$$\Phi_N(\Omega) = \frac{1}{N!} \sum_i K_i(A_i) A_i^{N-\gamma_i+1} \frac{\sec\theta^N}{E_\mu^{\gamma_i+N-1}} \times \int_0^1 G^N(x) x^{\gamma_i-2} e^{-\langle N \rangle} dx, \quad (15)$$

where N is the true multiplicity at the detector level and now the integration is over $x = E_\mu/(E_0/A)$ and $G(x)$ is

$$G(x) = 0.0145 x^{-0.757}(1 - x)^{5.25}.$$

5.1.2. Muon lateral spread

The lateral distribution of muons in a bundle around the shower axis directly determines the distortion effects on the observed multiplicity in a finite-size detector. For this reason we have to evaluate it very carefully. There are four factors [9] which influence muon spread: P_T distribution of the secondary mesons in high-energy collisions, muon generation height in the atmosphere, the deflection in the Earth's magnetic field and the multiple Coulomb scattering in the rock. It is not our purpose to see the details of these effects. But it is important to note that for our experimental site, at the large depth of ~ 3600 m.w.e. (meter water equivalent), the multiple scattering term far dominates on the magnetic field effect (an average deflection of $\langle R_{ms} \rangle \approx 2$ m compared to $\Delta x \approx 0.8$ m for the magnetic field).

We use, for the mean lateral spread, a parametrization from ref. (13), which gives

$$\langle r \rangle (E_0, A; > E_\mu) = A(E_\mu) + B(E_\mu) \left(\frac{E_\mu}{E}\right)^{0.62} \sec\theta, \quad (16)$$

where

$$A(E_\mu) = 3.13 E_\mu^{-0.46} \quad \text{and} \quad B(E_\mu) = 13.2 E_\mu^{-0.31}$$

(E_μ in TeV).

Eq. (16) holds in the assumption that the lateral spread depends only on the primary energy per nucleon and not on the event multiplicity.

The probability density of finding a muon at a distance r from the shower axis, on a plane parallel to the shower front, is well described by the exponential law

$$\rho(r) = \frac{1}{N} \frac{dN}{dr} = \frac{4r}{\langle r \rangle^2} e^{-2r/\langle r \rangle}, \quad (17)$$

and the function has been normalized to 1 on the interval $(0, \infty)$.

5.1.3. Folding in the detector

Once defined the real multiple muon flux at the depth of the detector, the next step is to fold in the apparatus taking into account all the experimental conditions (detector geometry, resolution and trigger logic).

The method which can be adopted in calculating the probability function $P_n(N)$ we have previously defined, strongly depends on the size of the detector compared to the typical muon lateral spread. The two simplest cases are the extreme ones:

- Infinite detector, which means $S \gg \pi\langle r\rangle^2$ (where S is the exposed area parallel to the shower front and $\langle r\rangle$ is the mean radius of the lateral muon distribution). This is the trivial case when no distortion occurs.
- Small-size detector, which means $S \ll \pi\langle r\rangle^2$. Muon density distribution can be assumed constant with a good approximation over the whole detector surface. A semianalytic calculation is easily accessible, as shown in ref. [15].

In our intermediate case the most complete method is through a Monte Carlo calculation. Our work proceeded essentially in two main steps:

(1) Calculating the "uncorrected" rates $R_N(A)$, as for the "infinite-detector" case, through the numerical integration of the real flux with the directional response function for the LVD box:

$$R_N(A) = \int \Phi_N(A, \Omega) S(\Omega)\, \mathrm{d}\Omega \quad \mathrm{s}^{-1}. \tag{18}$$

(2) Including the corrections to obtain the observed rates $R_n(A)$. For this purpose we have developed a Monte Carlo generator of multiple muon events and then calculated the probability $P_n(N, A)$ of detecting n muons in a bundle with multiplicity $N \geq n$ generated by a primary nucleus of mass A. The observed rates are then

$$R_n(A) = \sum_{N \geq n} R_N(A) P_n(N, A), \tag{19}$$

and summing over the five primary components we have

$$R_n = \sum_{N \geq n} R_N P_n(N), \tag{20}$$

with $R_N = \Sigma_A R_N(A)$ and $P_n(N)$ is now the probability of detecting n muons out of N in a bundle generated by any primary component.

This second step, for calculating the probability function, is certainly the most complicated work, due to the large number of parameters to be estimated and sensibly depending on each other. For the present analysis we generated samples of multiple muon events with multiplicity N in the range $N = 1, \ldots, 20$. For each event in a sample with fixed N (we analyzed samples of 3×10^4 events) we extract:

- average primary mass A with the weight function

$$R_N(A) = \int \Phi_N(A, \Omega) S(\Omega)\, \mathrm{d}\Omega; \tag{21}$$

- (θ, ϕ) direction with the weight

$$\Phi_N(A, \Omega) S(\Omega); \tag{22}$$

- primary nucleus energy E_0 with the weight

$$\frac{\mathrm{d}N}{\mathrm{d}E_0}(E_0, A) P_N(E_0, A, E_\mu(h(\Omega)), \theta); \tag{23}$$

- the ideal vertex of the shower axis with a uniform distribution on a "generation area" centered in the LVD box and orthogonal to the shower axis. In defining the generation area we have accurately evaluated the appropriate size and shape to not introduce any distortion in the muon lateral distribution (for more details see ref. [10]).
- the position of the N muons around the shower axis on the generation area with the density function (17). Each set of plane coordinates (x, y) is then converted to spatial coordinates (x', y', z') in the detector main reference system.

Events from all samples with at least one muon contained in the box are then selected. We impose a triggering condition (i.e. add an inefficiency factor in the detection of a single muon track) and count the observed number n of muons for each selected event.

We point out that the probability functions $P_n(N, A)$ and $P_n(N)$, as defined in eqs. (19) and (20), result from the convolution of two terms: the reduction factor due to the muon lateral separation, that reduces the observed number of muons in a bundle in a way dependent on the finite size of the exposed detector area, and the inefficiency factor in single track recording due to dead spaces and triggering requirements in the apparatus.

5.2. Rate prediction in the LVD

Our detector response was analyzed for three different trial compositions of the primary beam. We give a prediction of multiple muon rates observed assuming the two extreme models, the "Maryland spectrum" (MDI) and the "low energy composition" (LEC), and the NUSEX parametrization with two values of the spectral index of iron: $\gamma_{Fe} = 2.60$ and $\gamma_{Fe} = 2.70$.

5.2.1. Models for the primary composition

Assuming power law spectra as in eq. (11), each model predicts the values of spectral indices $\gamma_i(A)$ and coefficients $K_i(A)$ for the five primary components on the basis of different sets of experimental data. The relative contribution of iron nuclei at energies $\approx 10^{15}$ eV to the total composition drastically changes in the three models. We have considered:

- the NUSEX parametrization [4], with spectral index of 2.79 for protons and helium, 2.71 for CNO and Mg groups and in the range 2.60–2.70 for the iron group. All the details are included in table 2. Each component spectrum steepens to $\gamma_c = 3.0$ at a critical rigidity $R_c = 2 \times 10^6$ GeV/c. The break is at a total energy $E_c = (A/2)R_c$ for nuclei heavier than protons. We show in fig. 3 the integrated flux for each component.
- The "Maryland spectrum" (MDI), parametrized from measurements by Goodman et al. [16] on time arrival

Table 2
NUSEX parametrization for the primary cosmic-ray composition from ref. [4]; $(dN/dE) = K(A)E^{-\gamma(A)}$ and $(dN/dE)_c = K_c(A)E^{-3.0}$ cm^{-2} s^{-1} sr^{-1} (GeV/nucleon)$^{-1}$

Group	A	$K(A)$	$K_c(A)$	$\gamma(A)$
p	1	3.28	6.90×10^{1}	2.79
He	4	1.46×10^{-1}	2.66	2.79
CNO	14	6.80×10^{-3}	3.74×10^{-1}	2.71
Mg	28	3.10×10^{-3}	1.69×10^{-1}	2.71
Fe	56	3.83×10^{-4}	9.62×10^{-2}	2.60–2.70

Table 3
MDI parametrization for the primary cosmic-ray composition from ref. [16]; $(dN/dE) = K(A)E^{-\gamma(A)}$ and $(dN/dE)_c = K_c(A)E^{-3.0}$ cm^{-2} s^{-1} sr^{-1} (GeV/nucleon)$^{-1}$

Group	A	$K(A)$	$K_c(A)$	$\gamma(A)$
p	1	1.50	1.01×10^{2}	2.71
He	4	5.33×10^{-2}	2.93	2.71
CNO	14	3.62×10^{-3}	1.99×10^{-1}	2.71
Mg	28	1.14×10^{-3}	6.26×10^{-2}	2.71
Fe	56	1.30×10^{-4}	8.99×10^{-1}	2.36

distributions of energetic hadrons near air-shower cores. The spectral index for iron is 2.36, and for other nuclei 2.71. All spectra steepen to $\gamma_c = 3.0$ at a critical rigidity of 2×10^6 GeV/c. Because of the flatter spectrum of heavy nuclei they account for about 65% of the total above 2×10^6 GeV/nucleus. The parametrization used is shown in table 3.

- The "low energy compositions" (LEC) model, based on the extrapolation to high energies of the directly measured spectra at energies up to about 100 GeV/nucleon. The relative composition for the five groups is supposed to be constant at the same energy per nucleon in the following ratios [17]:

p : He : CNO : Mg : Fe = 1 : 0.035 : 0.0018 : 0.0005 : 0.00015.

Table 4
LEC parametrization for the primary cosmic-ray composition from ref. [18]; $(dN/dE) = K(A)E^{-\gamma(A)}$ and $(dN/dE)_c = K_c(A)E^{-3.0}$ cm^{-2} s^{-1} sr^{-1} (GeV/nucleon)$^{-1}$

Group	A	$K(A)$	$K_c(A)$	$\gamma(A)$
p	1	1.32	8.90×10^{1}	2.71
He	4	4.63×10^{-2}	2.55	2.71
CNO	14	2.38×10^{-3}	1.31×10^{-1}	2.71
Mg	28	6.62×10^{-4}	3.64×10^{-2}	2.71
Fe	56	1.99×10^{-4}	1.09×10^{-2}	2.71

The values for the parameters we use are those in table 4. We assume the same behaviour in the critical region as for MDI and NUSEX parametrizations.

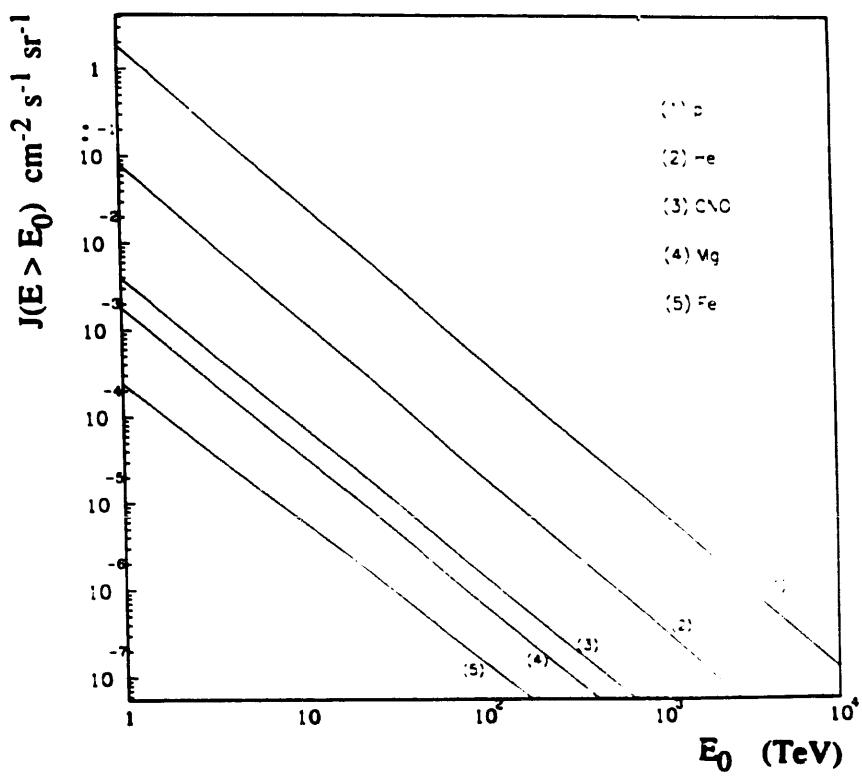

Fig. 3. The integrated flux of the five primary components (p, He, CNO, Si–Mg, Fe) at total energies $E_0 \geq 1$ TeV, with the NUSEX parametrization from ref. [4].

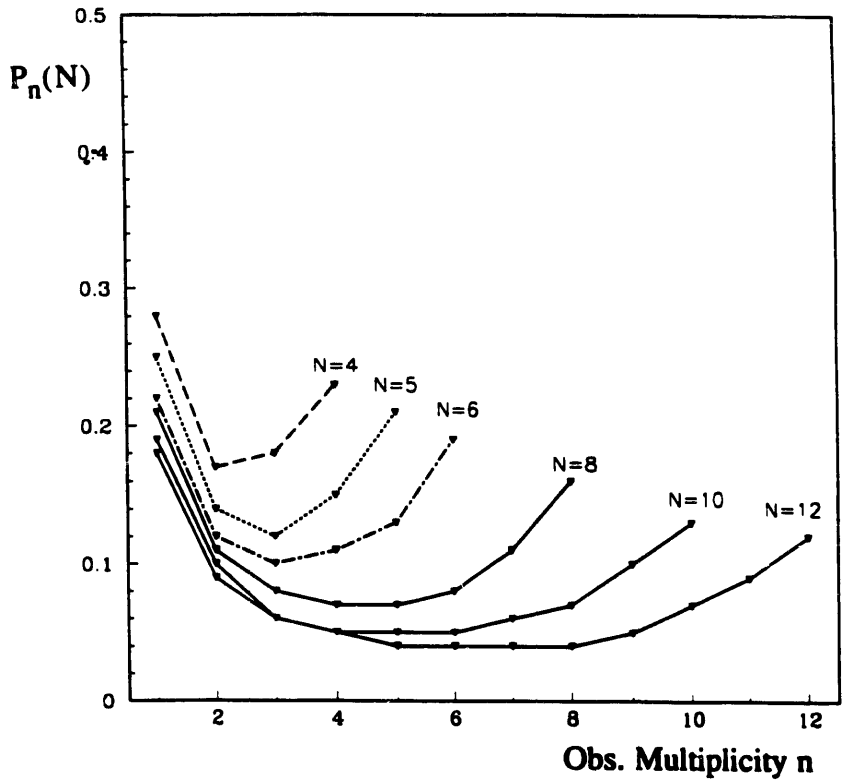

Fig. 4. The probability function $P_n(N)$ for multiplicities $N = 4, 5, 6, 8, 10, 12$.

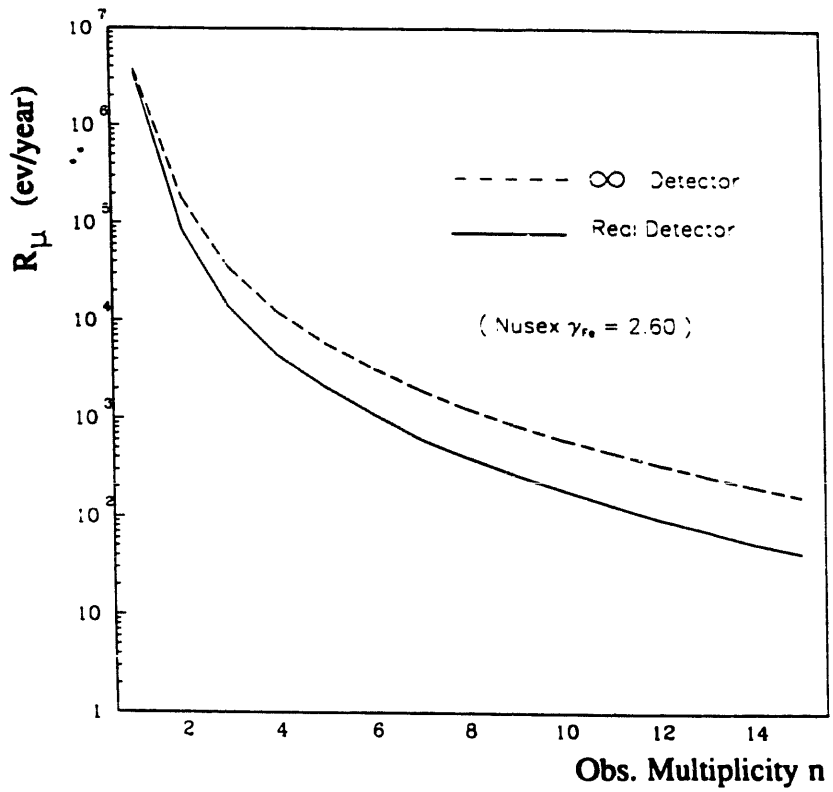

Fig. 5. The observed rates of multiple muon events in the "real" detector compared with the "infinite-detector" results. Predictions refer to the NUSEX model with $\gamma_{Fe} = 2.60$.

5.2.2. Results

For each model considered we have calculated three fundamental quantities through the Monte Carlo generation of samples of multiple muon events with fixed multiplicity:

- the "infinite-detector" rates $R_N(A)$ and R_N,
- the probability functions $P_n(N, A)$ and $P_n(N)$,
- the observed rates $R_n(A)$ and R_n.

For single track selection and recording, we have formulated a preliminary request imposing the passage through at least three geometrical planes (vertical or horizontal) extending over the full detector. The resultant efficiency factor is included in $P_n(N)$. Its behaviour, with the present assumptions, is shown in fig. 4 for some of the multplicities generated. Studying this function we have found that the shape of each curve strongly depends on the details of the detector geometry and the requests for single track detection.

Fig. 5 clearly shows how the finite size of the detector, together with trigger conditions, reduces the observed muon multiplicities in the apparatus. The two curves refer to the "infinite-detector" rates and the observed ones in the particular case of the NUSEX composition, with the spectral index of iron $\gamma_{Fe} = 2.60$.

A second effect is the decrease of the contribution of heavy nuclei to the number of muon groups at a given multiplicity, due to the fact that the lateral spread in a bundle increases with the mass of the primary component. On the other hand we can already note from this estimation the high capability of the detector in sampling high multiplicities. This is the direct effect of a large-area detector located at big depth.

Table 5
Ratios of multiples to singles in the detector, from simulation.

Model	R_2/R_1	R_4/R_1	R_6/R_1	R_8/R_1
MDI	0.0290	0.0022	0.0007	0.0003
NUSEX ($\gamma_{Fe} = 2.60$)	0.0248	0.0013	0.0003	0.0001
NUSEX ($\gamma_{Fe} = 2.70$)	0.0244	0.0011	0.0003	0.00006
LEC	0.0225	0.0008	0.0001	0.00005

To have a complete estimation of the sensitivity of the apparatus to the primary cosmic-ray composition we have compared event rate prediction for the three models assumed. MDI and LEC compositions bracket the values for the fraction of heavy nuclei we can expect. On the other hand NUSEX data give the most probable parametrization. Table 5 shows the ratios of multiple rates to single rates in the detector resulting from this simulation. In fig. 6 we show the final results.

The discrimination between the two extreme compositions is good. We can reach a good sensitivity in the region around multiplicity $n = 10$, where no observations are present up to now. What is more conclusive is the degree of sensitivity we have in discriminating a

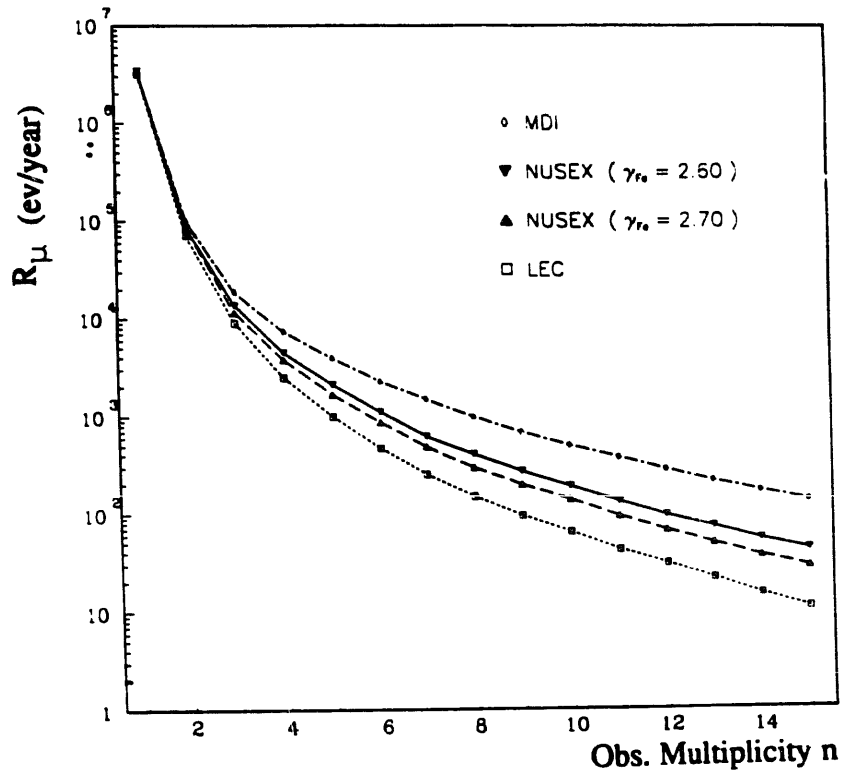

Fig. 6. Predictions for muon bundle rates in LVD as a function of the observed event multiplicity for different models of the primary composition.

variation $\Delta\gamma_{Fe} = 0.1$ for the NUSEX spectra. From the two curves we can obtain a 4σ separation for multiplicity $n = 10$ in one year of observation.

Acknowledgements

We would like to thank B. D'Ettorre Piazzoli and P. Lipari for many useful discussions concerning this work.

References

[1] H. Bilokon and V. Chiarella, Macro INT, memo: 24/88 LNF-INFN.
[2] B. Jeckelmann (LVD collaboration), Program GSASSD (4 November 1987).
[3] B. D'Ettorre Piazzoli, Le Rencontres de Physique de la Vallée d'Aoste, Supernova 1987A, one year later, ed. M. Greco (La Thuile, 1988) p. 239.
[4] G. Battistoni et al., ICRC La Jolla, OG session 5.1-5 (1986) p. 158.
[5] L. Bergamasco et al., Nuovo Cimento C6 (1983) 569.
[6] H.E. Bergesson et al., Proc. 13th Int. Conf. on Cosmic Rays, Denver 1973 (Colorado Associated University Press, Boulder, 1973) p. 1722.
[7] S. Miyake, J. Phys. Soc. Japan 18 (1963) 1093; M.R. Krishnaswamy et al., Phys. Lett. B27 (1968) 535.
[8] W.R. Sheldon et al., Phys. Rev. D17 (1978) 114.
[9] T.K. Gaisser and T. Stanev, Nucl. Instr. and Meth. A235 (1985) 183.
[10] E. Pallante, Thesis, University of Rome "La Sapienza" (April 1989).
[11] M. Basile et al., Some considerations on the LVD Tracking system trigger, LVD 041 (MEM) (September 1989).
[12] UA5 Collaboration, Z. Phys. C 43 (1989) 357; UA5 Collaboration, Proc. 17th Int. Symp. on Multiparticle Dynamics (Seewinkel, 1986) p. 553.
[13] G. Bologna et al., Nuovo Cimento C8 (1985) 76.
[14] G. Bologna et al., Nucl. Instr. and Meth. A234 (1985) 581.
[15] T.K. Gaisser and T. Stanev, Proc. Summer Workshop on Proton Decay Experiments, ed. D.S. Ayres (Argonne National Laboratory, 1982) p. 333.
[16] J.A. Goodman et al., Phys. Rev. Lett. 42 (1979) 854.
[17] J.W. Elbert, T.K. Gaisser and T. Stanev, Phys. Rev. D27 (1983) 1448.
[18] B. D'Ettorre Piazzoli, private communication.